

Quantum phase transitions in photonic cavities with two-level systems

M. I. Makin,¹ Jared H. Cole,¹ Charles Tahan,² Lloyd C. L. Hollenberg,¹ and Andrew D. Greentree¹
¹*Centre for Quantum Computer Technology, School of Physics, The University of Melbourne, Victoria 3010, Australia*
²*Cavendish Laboratory, University of Cambridge, JJ Thomson Ave, Cambridge CB3 0HE, United Kingdom*

(Received 23 November 2007; published 21 May 2008)

Systems of coupled photonic cavities have been predicted to exhibit quantum phase transitions by analogy with the Hubbard model. To this end, we have studied topologies of few (up to six) photonic cavities each containing a single two-level system. Quantum phase space diagrams are produced for these systems, and compared to mean-field results. We also consider finite effective temperature, and compare this to the notion of disorder. We find the extent of the Mott lobes shrink analogously to the conventional Bose-Hubbard model.

DOI: [10.1103/PhysRevA.77.053819](https://doi.org/10.1103/PhysRevA.77.053819)

PACS number(s): 42.50.Pq, 64.70.Tg, 03.67.-a

I. INTRODUCTION

There has recently been a convergence of several different fields of physics: condensed matter, quantum optics, and information science. This convergence has been realized by a staggering increase in the ability to fabricate and control quantum systems experimentally, and an ability to attack theoretical problems of increasing complexity. One aspect of this convergence of fields is the push to realize the quantum computer. Here we discuss another aspect: that of a quantum simulator. In particular, we explore the possibility for a quantum atomic-optical system (here an interacting lattice of optical cavities with embedded two-state systems) to undergo a quantum phase transition by direct analogy with the Hubbard model.

The Hubbard model [1] describes the hopping of interacting particles around a lattice of allowed positional states. A quantum phase transition is observed between delocalized particles (superfluid phase) and localized particles (Mott-insulator phase) depending on the strength of the hopping term relative to the on-site interaction. Numerous facets of the Hubbard model have been considered including the prediction of glassy phases [2], Hilbert-space optimization [3], and implementations of topological quantum computing [4]. One of the most dramatic and beautiful examples of the Bose-Hubbard model is the prediction [5] and recent demonstration [6] of the quantum phase transition in an ultracold atomic gas. Such demonstrations are significant for applying canonical solid-state treatments to the more controllable regime of atom optics, allowing new predictions to be tested (e.g., the supersolid phase [7]). Recent work on quantum phase transitions in photonic band-gap lattices does the same for the photonics-solid-state boundary [8–13].

At first glance, the possibility for a quantum phase transition in an optical system seems surprising. This is due to the fact that photons do not normally interact with each other with any appreciable strength, and for this reason most nonlinear optical processes are confined to the realm of classical optics. There are, however, many exceptions to this, but perhaps the most dramatic is the phenomenon of photon blockade [14]. Photon blockade is an example of a cavity quantum electrodynamical interaction in the strong coupling limit. An atom is placed in a cavity, and because the energy levels of the atom-cavity system depend on the number of photons in

the cavity, a photon-number-dependent resonance shift is observed [15]. If the atom-cavity interaction is strong enough, this shift can be sufficient to prevent more than a predetermined number of photons to enter the cavity: photon blockade. This effect has been analyzed for four-state systems [14,16,17] and two-state systems [18]. More recently photon blockade has been observed [19,20], adding substantial impetus to apply this effect to a range of applications.

Here we consider the properties of a lattice of cavities, each containing a single, quasis resonant two-state system, so as to be effectively treated by the Jaynes-Cummings interaction [21]. We go beyond the earlier idealized treatment [9] by building systems of increasing size to predict the results in the few-cavity (up to six) limit, and also consider the thermodynamic implications of disorder. By directly connecting these small scale cases (solved by direct diagonalization) with the thermodynamic limit, our results serve as a guide to coming proof-of-concept experiments. We are also able to compare our finite cases with the thermodynamic limit [9,11,22–26].

In Sec. II we introduce the system of coupled photonic blockade cavities that will be investigated for quantum phase transitions, and the extended Jaynes-Cummings-Hubbard Hamiltonians for both the exact calculation and for the mean-field approximation. In Sec. III we present results from the exact diagonalization techniques and compare with mean-field solutions. Finally, we consider disorder and the implications for effective model temperature in Sec. IV.

II. PHASE TRANSITIONS IN THE JAYNES-CUMMINGS-HUBBARD MODEL

The system under consideration is a lattice of optical cavities, each containing a single quasis resonant two-state system. The canonical treatment for a single atom-cavity system is the Jaynes-Cummings model. Photon hopping between cavities (which is effected by leakage out of the cavities, and into neighboring cavities) allows the direct comparison to Hubbard systems [27], and hence we refer to this as a Jaynes-Cummings-Hubbard (JCH) model. There are numerous ways in which to realize such a system depending on the available experimental configurations and desired topologies; for example, photonic band-gap structures [9] and coupled-cavity waveguides [10,12], perhaps realized in microfabricated dia-

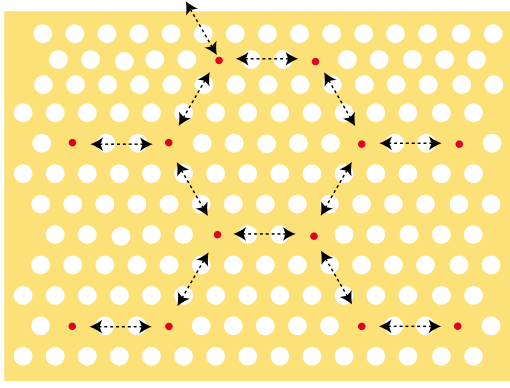


FIG. 1. (Color online) This schematic shows a possible implementation of the system, for three nearest neighbors. The dielectric medium is shown in yellow. The photonic crystal is made by periodic variations in refractive index, caused by drilling holes (white disks). The cavities are regions where holes have not been drilled—effectively, the undrilled holes. In each cavity, a red disk represents the two-level atom. The arrows indicate the nearest neighbors, across which photons can tunnel with hopping rate κ .

mond [28–30], arrays of superconducting strip-line cavities [31,32], or microcavities with individual cold atoms connected via optical fiber interconnects [33], or plasmonics [34]. For concreteness, we will focus our attention on a photonic band-gap structure where a two-dimensional array of photonic band-gap cavities constitutes the underlying lattice and defines the nearest-neighbor topology, and the two-state system is realized by an implanted impurity (Fig. 1).

Our emphasis in this work is on systems with a single two-state system per cavity, but it is important to note that this is not the only potential system for observing similar quantum phase transitions. Hartmann *et al.* have considered four-state systems [8,35], in keeping with the original Imamoglu proposal [14], whereas the case of many atoms per cavity has been considered by Na *et al.* [11]. The approach of Ref. [11] is particularly useful for providing a clear path to experiments using GaAs quantum dots.

To understand the properties of the JCH system, we first review the properties of the individual atom-cavity (Jaynes-Cummings) interactions. The Hamiltonian is

$$\mathcal{H}^{\text{JC}} = \epsilon\sigma^+\sigma^- + \omega a^\dagger a + \beta(\sigma^+ a + \sigma^- a^\dagger), \quad (1)$$

where σ^+ and σ^- (a^\dagger and a) correspond to the atomic (photonic) raising and lowering operators, respectively. The transition energy of the atomic system is ϵ , the cavity resonance is ω , and the cavity-mediated atom-photon coupling is β . The difference $\Delta = \omega - \epsilon$ is the detuning.

Let $|g, n\rangle$ ($|e, n\rangle$) ($n \in \mathbb{Z}^*$) represent a cavity that contains n photons and a single two-level atom in the ground (excited) state. The energy eigenvectors of Eq. (1) are given by $|g, 0\rangle$ and

$$|\pm, n\rangle = \frac{\beta\sqrt{n}|g, n\rangle + [-(\Delta/2) \pm \chi(n)]|e, n-1\rangle}{\sqrt{2\chi^2(n) \mp \chi(n)\Delta}} \quad \forall n \geq 1, \quad (2)$$

with eigenvalues

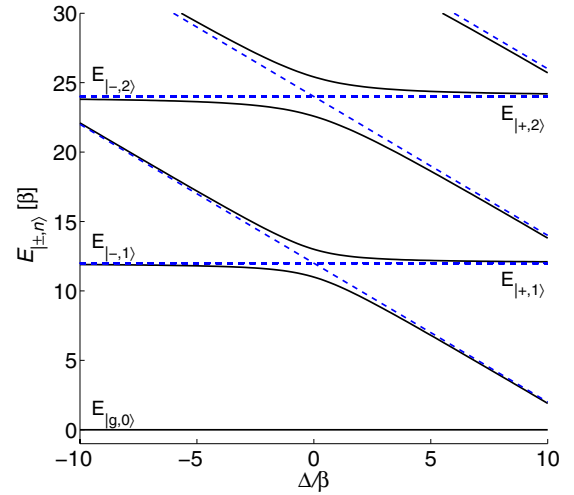


FIG. 2. (Color online) Energy eigenvalues [Eq. (3)] for a single cavity as a function of the detuning Δ . We set $\omega = 12\beta$ for illustrative purposes. The blue dashed lines indicate the asymptotes of the energies for each band, the diagonal lines represent the energy of the cavity due to the atom, while the horizontal lines represent the energy due to the photons only.

$$E_{|g, 0\rangle} = 0, \quad E_{|\pm, n\rangle} = n\omega \pm \chi(n) - \Delta/2, \quad (3)$$

where we have used the generalized Rabi frequency

$$\chi(n) = \sqrt{n\beta^2 + \Delta^2/4} \quad \forall n \geq 1 \quad (4)$$

where n is the total number of excitations. These eigenstates correspond to the well known dressed (polaritonic) states, and we call the basis formed by them the single-cavity dressed basis. The eigenspectrum of a single atom-cavity system is shown in Fig. 2. Because of the atom-photon-induced shift of the energy levels as a function of the number of excitations in the system, there is an effective photon-photon repulsion [18]. It is this photon-photon repulsion which plays the role of the on-site term in the Hubbard model, however, it is important to note that because the repulsion decreases with an increasing number of particles, the canonical Bose-Hubbard system is *not* realized in our case, and so although many qualitative similarities are predicted between the JCH and Bose-Hubbard models, exact equivalence is not guaranteed.

The nonbosonic nature of the particles in the Hamiltonian of Eq. (1) requires further discussion. Neither the JCH system nor the four-state system with few atoms per cavity [8] retrieve bosonic commutation relations. The limits where we can view the system as being comprised of interacting bosons are many atoms per cavity (holds for both the Jaynes-Cummings and four-state systems [8,11,36]), large detuning [9], and large excitation number. Arguably the most important case is that described here, namely, one atom per cavity with few excitations. This is because this regime maximizes the nonlinear (photon-photon) interactions, and is therefore the most experimentally accessible regime.

Differences between the JCH and Bose-Hubbard systems are interesting topics for investigation, and a study of the particle nature should prove fruitful, but goes beyond our

present work. We may understand some of the differences by comparing the on-site repulsion in the Bose-Hubbard and JCH cases. In the Bose-Hubbard system, the interaction U is a constant; however, in the JCH model this can be seen as having a particle number dependence, i.e., $U_{\pm}(n) = \pm [\chi(n+1) - \chi(n)]$. In the large photon limit, we obtain a noninteracting Bose gas, as $U_{\pm}(n) \rightarrow 0$, and in the large detuning limit, $U_{\pm}(n) \rightarrow \pm \beta^2/\Delta$, which is a constant bosonic Hubbard-type repulsion [11,36]. There is also no ideal Kerr-type term to generate an exact quartic interaction. Nonetheless, as has been shown, qualitative similarity between the phase diagrams of JCH and Bose-Hubbard systems is found, and the analysis of these phase diagrams is a major topic of this paper.

To generate the JCH Hamiltonian, we add hopping between cavities, and for a system of N cavities we have

$$\mathcal{H} = \sum_{i=1}^N \mathcal{H}_i^{\text{JC}} - \sum_{\langle i,j \rangle} \kappa_{ij} a_i^\dagger a_j, \quad (5)$$

where individual Jaynes-Cummings Hamiltonians of Eq. (1) have identical ϵ , ω , and β (this restriction will be relaxed later). The intercavity hopping occurs with frequency $\kappa_{ij} = \kappa$ for nearest neighbors, and $\kappa = 0$ otherwise; it is this term which defines the topology of the network. Photon transmission through a one-dimensional chain in a similar structure has also been considered [37].

To divine the properties of the phase transition seen in the thermodynamic limit, we introduce the operator that measures the total number of excitations of the system $\hat{L} = \sum_{i=1}^N \hat{L}_i$, where $\hat{L}_i = \sigma_i^+ \sigma_i^- + a_i^\dagger a_i$ is the number operator of atomic and photonic excitations of the i th cavity. One can include a term $-\mu \hat{L}$ in the Hamiltonian. We show below, through arguments of statistical mechanics, that μ represents the chemical potential. Section IV will continue into a discussion on effective model temperature and disorder. Let us include this chemical potential term in the Hamiltonian directly as follows:

$$\mathcal{H}' = \mathcal{H} - \mu \hat{L}. \quad (6)$$

We assume that the entire N -cavity system with l total excitations exists in the ground energy eigenstate $|\psi_g\rangle$, so that $\mathcal{H}'|\psi_g\rangle = E_g|\psi_g\rangle$ and $\hat{L}|\psi_g\rangle = l|\psi_g\rangle$ (i.e., these two operators commute).

To show that μ has the general form of a chemical potential, we begin with the usual definition of free energy $F = E - TS$, where E is the energy of the system \mathcal{H} (before chemical potential has been included), T is temperature and S is entropy. Assuming that $T=0$ and using the definition of chemical potential as the derivative of the free energy with respect to the number of excitations,

$$\mu \equiv \left(\frac{\partial F}{\partial l} \right)_{T,V} = \left(\frac{\partial E}{\partial l} \right)_{T,V}, \quad (7)$$

where l is used, as excitations act like particles in this system. We use the Hellmann-Feynman theorem [38,39] to cal-

culate the derivative of the energy with respect to number of excitations

$$\frac{\partial E}{\partial l} = \langle \psi_g | \frac{\partial \mathcal{H}}{\partial l} | \psi_g \rangle = \langle \psi_g | \frac{\partial}{\partial l} (\mathcal{H}' + \mu l) | \psi_g \rangle = \mu. \quad (8)$$

Hence the μ of Eq. (6) represents chemical potential as required.

The N -cavity bare basis consists of state vectors of the form $|s_1, n_1\rangle \otimes |s_2, n_2\rangle \otimes \cdots \otimes |s_N, n_N\rangle$, $s_i \in \{g, e\}$, $n_i \in \{0, 1, \dots\}$. In principle, this basis is infinite in extent, because the number of photonic excitations per cavity is unbounded. By ordering the bare basis by the *total* number of excitations (either photonic or atomic) across all cavities, one may express the Hamiltonian of Eq. (5) in block diagonal form $\mathcal{H} = \text{diag}[\mathcal{H}^{(0)}, \mathcal{H}^{(1)}, \mathcal{H}^{(2)}, \dots]$, where $\mathcal{H}^{(l)}$ is the matrix corresponding to l excitations. The size of each block is determined by the number of ways in which the excitations can be shared between the atomic and photonic degrees of freedom. We denote the number of states (equal to the size of the matrix $\mathcal{H}^{(l)}$) as s , where

$$s = \sum_{i=0}^{\min(l,N)} \binom{N}{i} S_{l-i}^N. \quad (9)$$

The above summation has two terms. $\binom{N}{i}$ is the total number of atomic excitations across the lattice (note that on each site the number of atomic excitations can only be zero or one). S_i^N represents the number of photonic excitations, and is the number of ways to share the $l-i$ photons between the N cavities (e.g., $S_2^3 = \text{length}[(2,0,0), (0,2,0), (0,0,2), (1,1,0), (1,0,1), (0,1,1)] = 6$).

To gain insight into the problem, we explicitly show $\mathcal{H}^{(0)}$ and $\mathcal{H}^{(1)}$ for a two-cavity system in the bare basis as follows:

$$\mathcal{H}^{(0)} = (0),$$

$$\mathcal{H}^{(1)} = \begin{pmatrix} \omega & \beta & -\kappa & 0 \\ \beta & \epsilon & 0 & 0 \\ -\kappa & 0 & \omega & \beta \\ 0 & 0 & \beta & \epsilon \end{pmatrix}, \quad (10)$$

where the (two-cavity) basis for $\mathcal{H}^{(0)}$ is $\{|g, 0, g, 0\rangle\}$ and for $\mathcal{H}^{(1)}$ is $\{|g, 1, g, 0\rangle, |e, 0, g, 0\rangle, |g, 0, g, 1\rangle, |g, 0, e, 0\rangle\}$.

To connect the finite case with the thermodynamic limit, we examine the phases of the N -cavity system \mathcal{H}' [Eq. (6)] as a function of ω , κ , and Δ . In particular, we are concerned with the expectation value of the total number of excitations of the system $\langle \hat{L} \rangle$. Note that \hat{L} is diagonal when represented in either the dressed or bare basis (but has different values in each). From [40], by subtracting $\mu \hat{L}$ from our Hamiltonian equation (5), we determine that $\langle \hat{L} \rangle = -\partial E_g / \partial \mu$, where E_g is the ground state energy of the *extended* Hamiltonian \mathcal{H}' . Some preliminary analytics can simplify the calculation of $\langle \hat{L} \rangle$ considerably; we show this now.

We begin by noting that the part of \hat{L} corresponding to exactly l excitations, represented as $\hat{L}^{(l)}$, has the very simple form

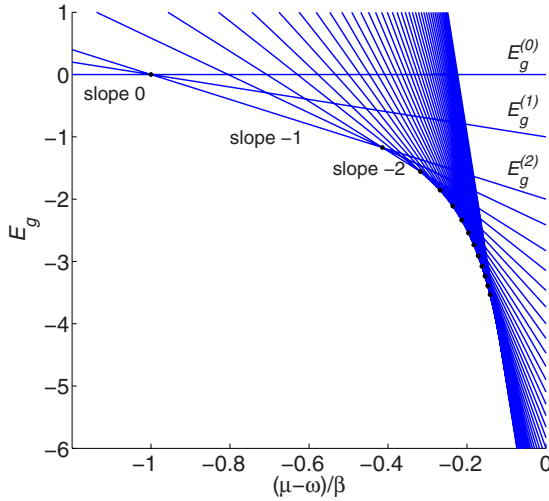


FIG. 3. (Color online) Ground state energies for each block of the Hamiltonian, Eq. (5), as a function of $(\mu-\omega)/\beta$, with $\kappa=0$. Recall that $\langle \hat{L} \rangle$ is equal to the negative of the slope (with respect to μ) of the smallest energy eigenvalue of the *whole* Hamiltonian, and that this slope is always an integer. This figure therefore shows explicitly how the phase diagrams are constructed—the black points indicate the boundaries between plateaus.

$$\hat{L}^{(l)} = lI. \quad (11)$$

Again employing the Hellmann-Feynman theorem,

$$\frac{\partial E_g^{(l)}}{\partial \mu} = \langle \psi_g | \frac{\partial}{\partial \mu} (\mathcal{H}^{(l)} - \mu lI) | \psi_g \rangle, \quad (12)$$

where $E_g^{(l)}$ is the ground state energy, and $|\psi_g\rangle$ is the corresponding eigenstate, of $\mathcal{H}^{(l)} - \mu \hat{L}^{(l)}$. This reduces to

$$\frac{\partial E_g^{(l)}}{\partial \mu} = -l. \quad (13)$$

So, if

$$M = \{ \min[\text{eigenvalues}(\mathcal{H}^{(0)} - \mu \hat{L}^{(0)})], \min[\text{eigenvalues}(\mathcal{H}^{(1)} - \mu \hat{L}^{(1)})], \dots \}, \quad (14)$$

and

$$f: \{0, 1, \dots\} \rightarrow M, \quad (15)$$

then

$$\langle \hat{L} \rangle = f^{-1}[\min(M)]. \quad (16)$$

In short, to find $\langle \hat{L} \rangle$, one simply needs to locate which block the minimum eigenvalue of $(\mathcal{H} - \mu \hat{L})$ corresponds to. Obviously, $\langle \hat{L} \rangle$ can only have non-negative integer values. This is illustrated further in Fig. 3. In this figure, the smallest eigenvalue of $\mathcal{H}^{(0)}, \mathcal{H}^{(1)}, \dots$ is plotted as a function of $(\mu-\omega)/\beta$ for $\kappa/\beta=0$. For each value, $\langle \hat{L} \rangle$ is given by the negative slope of the smallest eigenvalue at that point.

We now introduce the mean-field Hamiltonian. The mean-field approximation focuses attention on one particular cav-

ity, and assumes that its z nearest neighbors (that is, the coordination number is z) all behave like it. To invoke the mean field, we use the decoupling approximation $a_i^\dagger a_j = \langle a_i^\dagger \rangle a_j + \langle a_j \rangle a_i^\dagger - \langle a_i^\dagger \rangle \langle a_j \rangle$, and introduce the superfluid order parameter $\psi = \langle a_i \rangle = \langle a_i^\dagger \rangle$ (which we assume real), so that the Hamiltonian of Eqs. (5) and (6) becomes

$$\mathcal{H}^{\text{MF}} = \mathcal{H}^{\text{JC}} - z\kappa\psi(a^\dagger + a) + z\kappa\psi^2 - \mu \hat{L}. \quad (17)$$

The basis uses just one cavity, but the system (approximately) describes an infinite number. Note that the number of nearest neighbors z effectively “renormalizes” the mean-field coupling, i.e., $\kappa \rightarrow z\kappa$.

We have also considered using a larger unit cell—for example, using two cavities, each with z nearest neighbors. We found that while this is more difficult to calculate (finding eigenvalues of larger matrices) this exactly replicates the results of the original mean field—which is not surprising. However, this technique could be used to include disorder in the infinite cavity limit. Note that while Eq. (16) informs that the *total* number of excitations is integer, the mean-field Hamiltonian of Eq. (17) informs of the number of excitations *per cavity*. Accordingly, we will find equivalence when the number of excitations is a multiple of the number of cavities.

III. RESULTS

In this section we analyze the quantum phase diagram of the Hamiltonian of Eq. (5) for various topologies. Our analysis is based on exact diagonalization for up to six cavities. Topology is implemented through the κ_{ij} terms of Eq. (5). We then compare these topologies with the mean-field approximation.

We begin by considering the quantum phase diagrams of the exact systems. We display the phase diagrams corresponding to two, three, four, and five cavities arranged in one dimension with periodic boundary conditions in Fig. 4. Each color corresponds to a different plateau, a constant state in excitation space—these are Mott insulating phases. It is worth pointing out that in our discrete model, no superfluid phase exists. However, for significantly large κ , the plateaus get closer together, approximating the superfluid phase diagram, as in the mean-field case.

In total, 11 topologies were examined. These are listed in the first column of Table I. The topologies of a square, triangle, and six cavities with $z=3$ could be considered special, as they can represent infinite square, triangular, and hexagonal lattices, respectively. However, no significant differences (with respect to matching of phase diagrams to mean field) are found between these topologies and the rest.

For all topologies, a “pinch” effect is noted as $\kappa \rightarrow 0$ between $\langle \hat{L} \rangle = N$ and $\langle \hat{L} \rangle = 2N$, between $\langle \hat{L} \rangle = 2N$ and $\langle \hat{L} \rangle = 3N$, etc. That is, all fractional occupations (plateaus corresponding to heights that are *not* integer multiples of the number of cavities N) disappear as $\kappa \rightarrow 0$; this compares nicely with the mean-field solution. The point at which this pinching occurs is called the critical chemical potential μ_c . We find

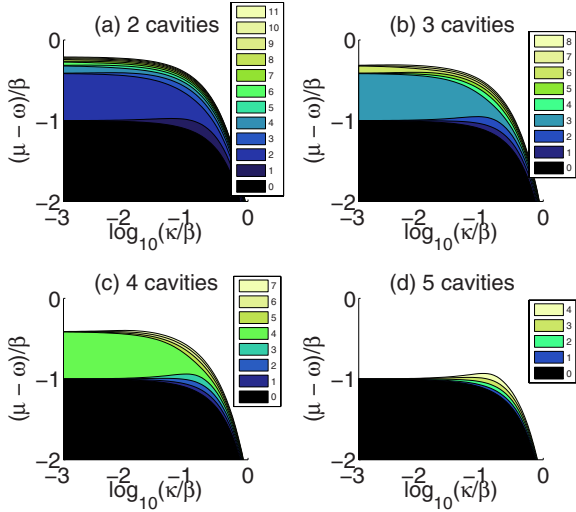


FIG. 4. (Color online) These plots show the expectation value of the total number of excitations $\langle \hat{L} \rangle$ as a function of $(\mu - \omega)/\beta$ and $\log_{10}(\bar{\kappa}/\beta)$, for two, three, four, and five cavities in periodic boundary conditions, with $\Delta=0$. Note that the top boundary in each plot is the limit of calculations. The Hamiltonian matrix used to create each plot is truncated at $l=12, 9, 8,$ and $5,$ respectively.

$$\mu_c(n) = \omega + \chi(n) - \chi(n+1), \quad (18)$$

where $\chi(n)$ is defined in Eq. (4), and $\chi(0)=-\Delta/2$. This is independent of the number or arrangement of cavities, and independent of whether or not the mean-field approximation is used, as expected from the $\kappa \rightarrow 0$ limit.

Although in general, one cannot analytically determine the positions of all the boundaries, we find that for all topologies, the first boundary (between $\langle \hat{L} \rangle=0$ and $\langle \hat{L} \rangle=1$) is described by the analytic equation

$$\frac{\mu - \omega}{\beta} = -\frac{1}{2} \left[\frac{\Delta + z\kappa}{\beta} + \sqrt{\left(\frac{\Delta - z\kappa}{\beta} \right)^2 + 4} \right], \quad (19)$$

where z is the number of nearest neighbors (the third column in Table I). Equation (19) was determined by equating the smallest eigenvalue of $\mathcal{H}^{(1)}$ with zero (the only eigenvalue of $\mathcal{H}^{(0)}$). This has been compared numerically for $z=1, 2, 3, 4, 6$ and is in excellent agreement. One cannot expect generic z analytic boundaries between $\langle \hat{L} \rangle=1$ and $\langle \hat{L} \rangle=2$ or higher to exist; indeed, none were determined. This is because they are truly in the realm of many-body physics (unlike the lower boundary). A higher boundary would be the solution of a commensurately higher order polynomial. In the simplest case, $N=2$ and $l=2$, from Eq. (9), $s=8$, so an eighth order polynomial must be solved to determine the boundaries.

For each plateau, the ground eigenstate can be calculated (hence below we use ‘‘ground eigenstates’’ to refer to the different ground states for the different plateaus). These ground eigenstates are represented in the dressed state basis, even though many of the calculations above were done in the bare basis.

To easily represent this information, it is useful to define two operators: the translation operator \hat{T} (which shifts states to the right and moves the last state back to the beginning) and the permutation operator \hat{P}_m (which is the sum over \hat{T}^i applied to the state m times),

$$\begin{aligned} & \hat{T}(|s_1, n_1\rangle \otimes \cdots \otimes |s_{N-1}, n_{N-1}\rangle \otimes |s_N, n_N\rangle) \\ & = |s_N, n_N\rangle \otimes |s_1, n_1\rangle \otimes \cdots \otimes |s_{N-1}, n_{N-1}\rangle, \end{aligned} \quad (20)$$

$$\begin{aligned} \hat{P}_m(|s_1, n_1\rangle \otimes \cdots \otimes |s_N, n_N\rangle) & = \sum_{i=0}^{m-1} (\hat{T})^i (|s_1, n_1\rangle \otimes \cdots \\ & \otimes |s_N, n_N\rangle). \end{aligned} \quad (21)$$

The ground eigenstates for all 11 topologies, up to $\langle \hat{L} \rangle=N$, i.e., total number of excitations equal to number of cavities, are displayed in Table I. See Fig. 5 for a diagrammatical example of how, for two cavities, the information from the table matches a phase diagram.

Consider bands labeled by m , where

$$mN \leq \langle \hat{L} \rangle \leq (m+1)N - 1 \quad \forall \quad m=0, 1, \dots \quad (22)$$

One finds that the physics of each band has some striking similarities, hence the introduction of this parameter.

In Table I only results for $m=0$ are displayed. While higher bands include many more possible states (e.g., $|-, 1\rangle \otimes |+, 1\rangle \otimes |-, 2\rangle$), we find higher bands have a surprisingly simple structure. To obtain the general states for some other band m , one needs to simply replace $|-, 1\rangle$ by $|-, m+1\rangle$, and $|g, 0\rangle$ by $|-, m\rangle$, in every instance.

The differences between topologies are apparent when comparing, for example, the band $m=0$, for $2 \leq \langle \hat{L} \rangle \leq N-1$, two excitations in a square topology compared with two excitations in a tetrahedron topology. In the square case, there is a different coefficient for excitations adjacent as to excitations separated, compared with the tetrahedron case, where all terms have the same coefficient.










Three different topologies (pentagon, six cavities with $z=3$, and six cavities with $z=4$) have some coefficients displayed to three decimal places; these have been calculated to 12 decimal places. An exact form is not derived; as these numbers represent solutions of polynomials of order ≥ 50 no exact form is necessarily expected.

We also examine the expectation value of the number of excitations of each cavity, $\langle \hat{L}_i \rangle$ and $\langle \hat{L}_i^2 \rangle$, and find that, independent of topology,

$$\langle \hat{L}_i \rangle = \frac{\langle \hat{L} \rangle}{N},$$

$$\langle \hat{L}_i^2 \rangle = (m+1)^2 \left(\frac{\langle \hat{L} \rangle - mN}{N} \right) + m^2 \left(1 - \frac{\langle \hat{L} \rangle - mN}{N} \right), \quad (23)$$

TABLE I. Summary of information about the number of cavities N , and nearest neighbors z , excitation state $\langle \hat{L} \rangle$, and associated ground eigenstate for 11 topologies up to $N=6$ for the band $m=0$. Eigenstates for higher bands m are determined by replacing $|g, 0\rangle$ and $|-, 1\rangle$ by $|-, m+1\rangle$ in every instance. The first four rows are valid for any topology.

Topology	N	z	$\langle \hat{L} \rangle$	Associated ground eigenstate (dressed basis)
Arbitrary	n	N/A	0	$ g, 0\rangle^{\otimes n}$
Arbitrary	n	N/A	1	$\frac{1}{\sqrt{n}} \hat{P}_n(g, 0\rangle^{\otimes(n-1)} \otimes -, 1\rangle)$
Arbitrary	n	N/A	$n-1$	$\frac{1}{\sqrt{n}} \hat{P}_n(g, 0\rangle \otimes -, 1\rangle^{\otimes(n-1)})$
Arbitrary	n	N/A	n	$ -, 1\rangle^{\otimes n}$
	2	1	1	$\frac{1}{\sqrt{2}} \hat{P}_2(g, 0\rangle \otimes -, 1\rangle)$
	4	2	2	$\frac{1}{\sqrt{8}} \hat{P}_4(g, 0\rangle^{\otimes 2} \otimes -, 1\rangle^{\otimes 2}) + \frac{1}{2} \hat{P}_2[(g, 0\rangle \otimes -, 1\rangle)^{\otimes 2}]$
	4	3	2	$\frac{1}{2} \{ \hat{P}_4(g, 0\rangle^{\otimes 2} \otimes -, 1\rangle^{\otimes 2}) + \hat{P}_2[(g, 0\rangle \otimes -, 1\rangle)^{\otimes 2}] \}$
	5	2	2	$0.235 \hat{P}_5(g, 0\rangle^{\otimes 3} \otimes -, 1\rangle^{\otimes 2}) + 0.380 \hat{P}_5(g, 0\rangle^{\otimes 2} \otimes -, 1\rangle \otimes g, 0\rangle \otimes -, 1\rangle)$
			3	$0.235 \hat{P}_5(g, 0\rangle^{\otimes 2} \otimes -, 1\rangle^{\otimes 3}) + 0.380 \hat{P}_5(g, 0\rangle \otimes -, 1\rangle \otimes g, 0\rangle \otimes -, 1\rangle^{\otimes 2})$
	5	4	2	$\frac{1}{\sqrt{5}} \{ \hat{P}_5(g, 0\rangle^{\otimes 3} \otimes -, 1\rangle^{\otimes 2}) + \hat{P}_5(g, 0\rangle^{\otimes 2} \otimes -, 1\rangle \otimes g, 0\rangle \otimes -, 1\rangle) \}$
			3	$\frac{1}{\sqrt{5}} \{ \hat{P}_5(g, 0\rangle^{\otimes 2} \otimes -, 1\rangle^{\otimes 3}) + \hat{P}_5(g, 0\rangle \otimes -, 1\rangle \otimes g, 0\rangle \otimes -, 1\rangle^{\otimes 2}) \}$
	6	2	2	$\frac{1}{6} \hat{P}_6(g, 0\rangle^{\otimes 4} \otimes -, 1\rangle^{\otimes 2}) + \frac{1}{\sqrt{12}} \hat{P}_6(g, 0\rangle^{\otimes 3} \otimes -, 1\rangle \otimes g, 0\rangle \otimes -, 1\rangle) + \frac{1}{3} \hat{P}_3[(g, 0\rangle^{\otimes 2} \otimes -, 1\rangle)^{\otimes 2}]$
			3	$\frac{1}{\sqrt{72}} \hat{P}_6(g, 0\rangle^{\otimes 3} \otimes -, 1\rangle^{\otimes 3}) + \frac{1}{\sqrt{18}} \hat{P}_6(g, 0\rangle^{\otimes 2} \otimes -, 1\rangle \otimes g, 0\rangle \otimes -, 1\rangle^{\otimes 2}) + g, 0\rangle^{\otimes 2} \otimes -, 1\rangle^{\otimes 2} \otimes g, 0\rangle \otimes -, 1\rangle + \frac{1}{\sqrt{8}} \hat{P}_2[(g, 0\rangle \otimes -, 1\rangle)^{\otimes 3}]$
			4	$\frac{1}{6} \hat{P}_6(g, 0\rangle^{\otimes 2} \otimes -, 1\rangle^{\otimes 4}) + \frac{1}{\sqrt{12}} \hat{P}_6(g, 0\rangle \otimes -, 1\rangle \otimes g, 0\rangle \otimes -, 1\rangle^{\otimes 3}) + \frac{1}{3} \hat{P}_3[(g, 0\rangle \otimes -, 1\rangle^{\otimes 2})^{\otimes 2}]$
	6	3	2	$\frac{1}{\sqrt{18}} \{ \hat{P}_6(g, 0\rangle^{\otimes 4} \otimes -, 1\rangle^{\otimes 2}) + \hat{P}_3(g, 0\rangle^{\otimes 2} \otimes -, 1\rangle)^{\otimes 2} \} + \frac{1}{\sqrt{12}} \hat{P}_6(g, 0\rangle^{\otimes 3} \otimes -, 1\rangle \otimes g, 0\rangle \otimes -, 1\rangle)$
			3	$0.208 \hat{P}_6(g, 0\rangle^{\otimes 3} \otimes -, 1\rangle^{\otimes 3}) + g, 0\rangle^{\otimes 2} \otimes -, 1\rangle \otimes g, 0\rangle \otimes -, 1\rangle^{\otimes 2} + g, 0\rangle^{\otimes 2} \otimes -, 1\rangle^{\otimes 2} \otimes g, 0\rangle \otimes -, 1\rangle + 0.334 \hat{P}_2[(g, 0\rangle \otimes -, 1\rangle)^{\otimes 3}]$
			4	$\frac{1}{\sqrt{18}} \{ \hat{P}_6(g, 0\rangle^{\otimes 2} \otimes -, 1\rangle^{\otimes 4}) + \hat{P}_3(g, 0\rangle \otimes -, 1\rangle^{\otimes 2})^{\otimes 2} \} + \frac{1}{\sqrt{12}} \hat{P}_6(g, 0\rangle \otimes -, 1\rangle \otimes g, 0\rangle \otimes -, 1\rangle^{\otimes 3})$
	6	4	2	$0.246 \hat{P}_6(g, 0\rangle^{\otimes 4} \otimes -, 1\rangle^{\otimes 2}) + g, 0\rangle^{\otimes 3} \otimes -, 1\rangle \otimes g, 0\rangle \otimes -, 1\rangle + 0.304 \hat{P}_3[(g, 0\rangle^{\otimes 2} \otimes -, 1\rangle)^{\otimes 2}]$
			3	$0.197 \{ \hat{P}_6(g, 0\rangle^{\otimes 3} \otimes -, 1\rangle^{\otimes 3}) + \hat{P}_2[(g, 0\rangle \otimes -, 1\rangle)^{\otimes 3}] \} + 0.240 \hat{P}_6(g, 0\rangle^{\otimes 2} \otimes -, 1\rangle \otimes g, 0\rangle \otimes -, 1\rangle^{\otimes 2}) + g, 0\rangle^{\otimes 2} \otimes -, 1\rangle^{\otimes 2} \otimes g, 0\rangle \otimes -, 1\rangle$
			4	$0.246 \hat{P}_6(g, 0\rangle^{\otimes 2} \otimes -, 1\rangle^{\otimes 4}) + g, 0\rangle \otimes -, 1\rangle \otimes g, 0\rangle \otimes -, 1\rangle^{\otimes 3} + 0.304 \hat{P}_3[(g, 0\rangle \otimes -, 1\rangle^{\otimes 2})^{\otimes 2}]$
	6	5	2	$\frac{1}{\sqrt{15}} \{ \hat{P}_6(g, 0\rangle^{\otimes 4} \otimes -, 1\rangle^{\otimes 2}) + g, 0\rangle^{\otimes 3} \otimes -, 1\rangle \otimes g, 0\rangle \otimes -, 1\rangle + \hat{P}_3[(g, 0\rangle^{\otimes 2} \otimes -, 1\rangle)^{\otimes 2}] \}$
			3	$\frac{1}{\sqrt{20}} \{ \hat{P}_6(g, 0\rangle^{\otimes 3} \otimes -, 1\rangle^{\otimes 3}) + g, 0\rangle^{\otimes 2} \otimes -, 1\rangle \otimes g, 0\rangle \otimes -, 1\rangle^{\otimes 2} + g, 0\rangle^{\otimes 2} \otimes -, 1\rangle^{\otimes 2} \otimes g, 0\rangle \otimes -, 1\rangle + \hat{P}_2[(g, 0\rangle \otimes -, 1\rangle)^{\otimes 3}] \}$
			4	$\frac{1}{\sqrt{15}} \{ \hat{P}_6(g, 0\rangle^{\otimes 2} \otimes -, 1\rangle^{\otimes 4}) + \hat{P}_3[(g, 0\rangle \otimes -, 1\rangle^{\otimes 2})^{\otimes 2}] + \hat{P}_6(g, 0\rangle \otimes -, 1\rangle \otimes g, 0\rangle \otimes -, 1\rangle^{\otimes 3}) \}$

so that the variance of \hat{L}_i is

$$\text{var}(\hat{L}_i) = \sqrt{\langle \hat{L}_i^2 \rangle - \langle \hat{L}_i \rangle^2} = \sqrt{\frac{\langle \hat{L} \rangle - mN}{N} - \left(\frac{\langle \hat{L} \rangle - mN}{N} \right)^2}, \quad (24)$$

where the band m is defined by Eq. (22), and both Eqs. (23) and (24) are valid for $i=1, \dots, N$. From this, one can determine that if $\langle \hat{L} \rangle$ is an integer multiple of N , $\text{var}(\hat{L}_i)=0$, as expected. Also, if we consider the thermodynamic limit, where both the number of cavities and the number of excitations approach infinity ($N \rightarrow \infty, \langle \hat{L} \rangle \rightarrow \infty$), while the excita-

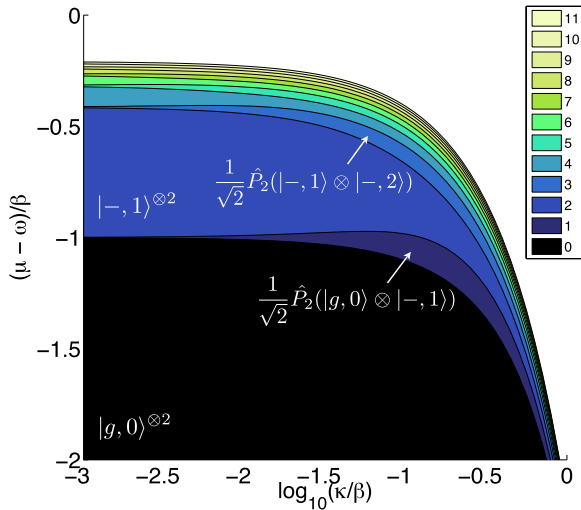


FIG. 5. (Color online) The expectation value of the total number of excitations $\langle \hat{L} \rangle$ of two cavities with periodic boundary conditions in the ground state. The eigenstates of the four lowest plateaus are marked (see Table I). The upper boundary marks the limit of calculations.

tion density remains constant at $\rho = \langle \hat{L} \rangle / N$, we find that $\text{var}(\hat{L}_i) \rightarrow 0$.

While this paper primarily focuses on phase changes as a function of κ , one can also examine phase changes as a function of detuning Δ [12]. Indeed, experimentally shifts in Δ may prove to be more accessible (via the Stark shift), as κ cannot be changed postfabrication in many systems. In Fig. 6(a) we plot $\langle \hat{L} \rangle$ as a function of Δ/β and $(\mu - \omega)/\beta$ for $\kappa = 0$, and in Fig. 6(b) we do the same for $\kappa = 10^{-1/2}\beta$. There are fewer plateaus in (a) than there are in (b) because there are fewer plateaus (due to the pinching effect, discussed above) at $\kappa/\beta = 0$. Note the *symmetry* around $\Delta = 0$, in the

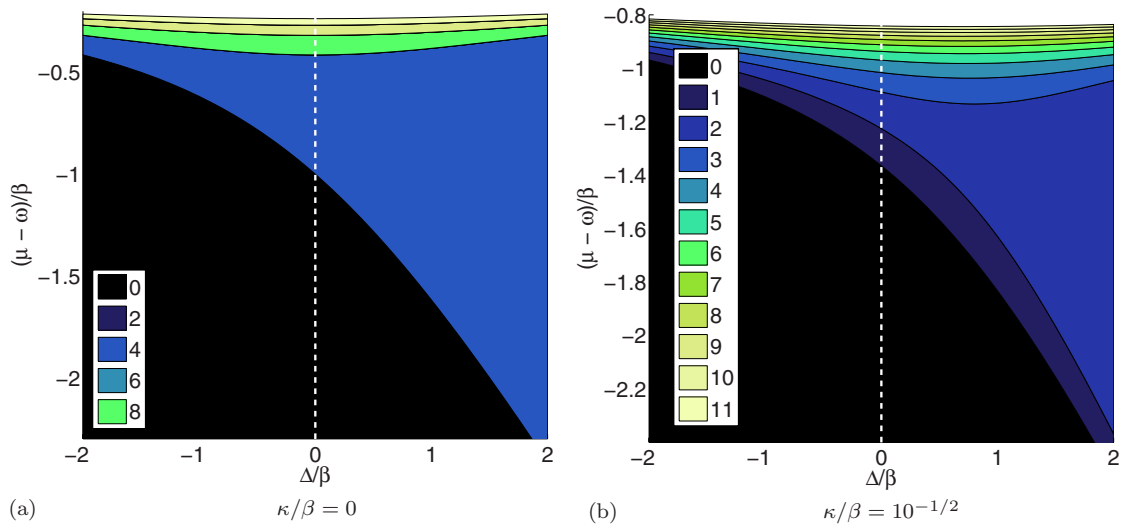


FIG. 6. (Color online) These plots show $\langle \hat{L} \rangle$ as a function of $(\mu - \omega)/\beta$ and Δ/β for two cavities in periodic boundary conditions with (a) $\kappa = 0$ and (b) $\kappa = 10^{-1/2}\beta$. The upper boundary in both cases marks the limit of calculations. Note that only even plateaus are present in (a). This is because of the pinching effect as $\kappa \rightarrow 0$ —in this limit, plateaus corresponding to fractional occupation do not exist. The white dashed line marks $\Delta/\beta = 0$, and aids the eye in seeing that the boundaries above the first (second) are symmetric (asymmetric) in plot (a) [(b)].

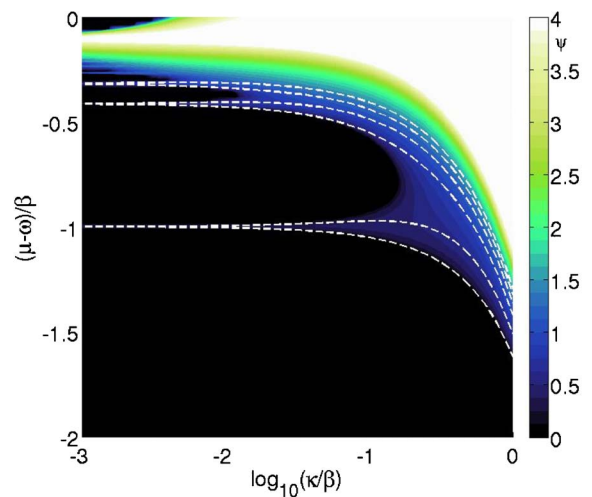


FIG. 7. (Color online) This plot shows the mean-field result for $z=1$, overlaid with the exact cavity results for two cavities with one connection (white dashed lines), as in the fifth row of Table I. Note the excellent agreement between exact results and mean-field approximation.

second and subsequent boundaries of Fig. 6(a) (cf. Fig. 3 of [9]), and the corresponding *asymmetry* in the third and subsequent boundaries of Fig. 6(b). This symmetry is perfect at $\kappa = 0$, and the asymmetry increases with increasing κ .

A mean-field phase diagram that is comparable with the phase diagrams of the previous section can be made [9]. An accurate comparison between the exact results of the previous section, with mean field, is made when we consider topologies with z nearest neighbors with mean-field results for z nearest neighbors. In all 11 distinct topologies tested, a very accurate match is seen. One such result is displayed in Fig. 7. We find that the boundaries from Eq. (18) are preserved in the mean-field solutions.

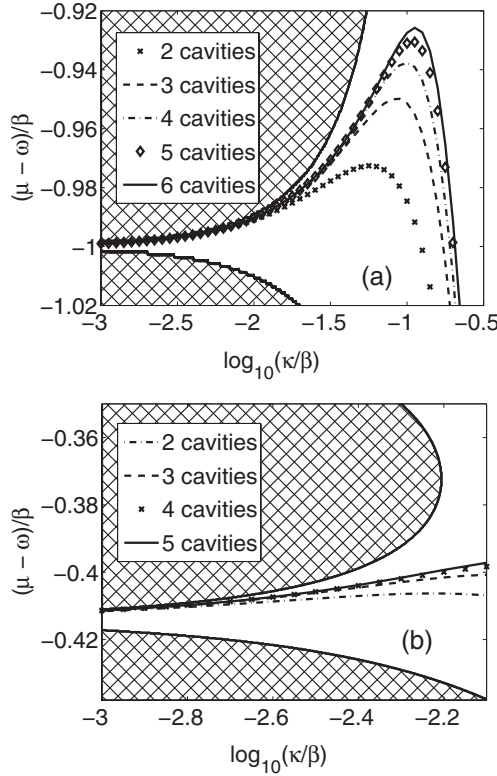


FIG. 8. The hatched region represents the $\psi=0$ area of the mean-field approximation for two nearest neighbors. The lines (or markers, for distinction purposes only) represent the exact calculations. (a) shows the boundary between the zeroth and first lobe, and (b) shows the boundary between the first and second lobe. Note that as the number of cavities increases, the lines tend to hug the upper mean-field lobe. This indicates qualitatively that as $N \rightarrow \infty$, the exact calculations should approach the mean-field ($N = \infty$) limit.

In mean field, the region with $\psi=0$ corresponds to the various Mott insulating lobes (e.g., $|g, 0\rangle$, $|-1, 1\rangle$, $|-2, 2\rangle$, etc.), while $\psi > 0$ is the superfluid state. The bottom lobe is described as the zeroth lobe ($|g, 0\rangle$), the next lobe up as the first lobe ($|-1, 1\rangle$), and so on. In Fig. 8(a), we examine the underside of the first lobe in mean field with $z=2$, and overlay the boundary between $\langle \hat{L} \rangle = N-1$ and $\langle \hat{L} \rangle = N$ for $N=2, 3, 4, 5$, and 6 cavities in periodic boundary conditions. In Fig. 8(b), we examine the underside of the second lobe in mean field with $z=2$, and plot the boundary between $\langle \hat{L} \rangle = 2N-1$ and $\langle \hat{L} \rangle = 2N$ for $N=2, 3, 4, 5$ cavities, also in periodic boundary

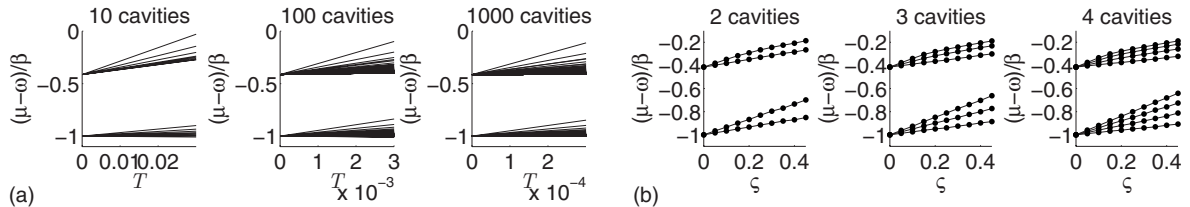


FIG. 9. (a) shows how the boundaries between plateaus change (when $\kappa=0$) for 10, 100, and 1000 cavities with increasing temperature in natural units. (b) shows how the boundaries between plateaus change (when $\kappa=0$) for two, three, and four cavities with increasing disorder, measured in units of standard deviation ς . Note that when $\varsigma=0.4$, the difference between the top line of the bottom “pinch,” and the bottom line of the top pinch, is $(\mu - \omega)/\beta = 0.434, 0.361,$ and 0.320 for two, three, and four cavities, respectively. This gives some indication of a threshold of tolerance.

conditions. One can clearly see how as the number of cavities increases, the boundaries approach the boundary of mean field, and eventually may pinch off for each lobe entirely (so that plateaus of height $\langle \hat{L} \rangle / N = 1, 2, \dots$ do not continue as $\kappa \rightarrow \infty$, but rather have finite size in this direction). These boundaries accord well with the structures observed by Rosario and Fazio (Fig. 3 of Ref. [10]) which were obtained independently by the density matrix renormalization group procedure, which lends weight to both quantum treatments. Furthermore, as $N \rightarrow \infty$, our exact results approach that of the mean field, which have a more rounded cutoff for the Mott lobes than these finite cavity results.

IV. DISORDER AND EFFECTIVE MODEL TEMPERATURE

In this section, we first consider the modification of the chemical potential with small temperature increase (less than the scale for photon generation, $kT \ll \hbar\omega$) and hence this modifies the phase diagrams above. We then examine fabrication disorder in the form of a normal distribution of photon energies for each cavity. We show that this fabrication disorder is qualitatively similar to effective temperature, providing a connection between disorder and an effective temperature in this analog system.

Note that we set Boltzmann’s constant $k_B = 1$. We begin by differentiating the free energy $F = E - TS$ with respect to the total number of excitations l ,

$$\frac{\partial F}{\partial l} = \frac{\partial E}{\partial l} - T \frac{\partial S}{\partial l} - S \frac{\partial T}{\partial l}, \quad (25)$$

recalling the definition of chemical potential in Eq. (7), and assuming that temperature does not depend on the number of excitations (i.e., $\partial T / \partial l = 0$, assuming that the temperature scale is too low to generate a photon, i.e., $kT \ll \hbar\omega$), we get

$$\mu = \frac{\partial E}{\partial l} + T \frac{\partial S}{\partial l}. \quad (26)$$

This then gives an effective chemical potential

$$\mu' = \mu + T \frac{\partial S}{\partial l}. \quad (27)$$

We calculate the entropy S in the $\kappa \rightarrow 0$ limit in the following manner. Assume that the photon blockade is complete, i.e., $|-2, g, 0\rangle \leftrightarrow |-1, -, 1\rangle$, then we can consider each band [re-

call Eq. (22)] separately. More specifically, each band acts like a paramagnet [41]. Recall that a one-dimensional paramagnet is a line of spin states, where each spin can point up or down. Compare with our system, where each cavity can have either $|g, 0\rangle$, or $|-1\rangle$ (for band $m=0$). Strictly speaking, each state (as in Table I) is a pure state, and as such the entropy is zero. However, if we assume that the number of cavities N is very large, then the superposition states acts like a mixed state, and we can define entropy as for a paramagnet (essentially the logarithm of the number of microstates) by

$$S(l) = \ln \binom{N}{l - mN}. \quad (28)$$

Note that this solution is only valid within each band, and as such we can ignore the infinities that arise in $\partial S / \partial l$ when l is an integer multiple of N , as at these points the paramagnetic approximation does not apply. Recall that the phase diagram of $\langle \hat{L} \rangle$ is concerned with finding the slope of the smallest energy eigenvalue with respect to μ , and that this slope is always an integer. The Hamiltonian of Eq. (5) is block diagonal. We know from earlier analysis that the ground state energy of each block $\mathcal{H}^{(l)}$ has constant slope with respect to μ of $-l$. Consider Fig. 3: when temperature is included, each line will move, with respect to $(\mu - \omega) / \beta$ by some amount to the left or to the right. For each μ , we choose the smallest energy eigenvalue at that point, and take the negative slope at that point. For small finite temperatures, this is manifest as a “splitting” of the pinches, as seen in [2]. We plot this splitting between the zeroth and first lobes, and the first and second lobe, for $N=10, 100, 1000$ in Fig. 9(a).

Fabrication of a system of photonic cavities will undoubtedly be subject to certain errors. Here we model uncertainty in the cavity frequency ω . We assume that each cavity may be tuned individually to $\Delta_i = 0 \quad \forall \quad i=1, \dots, N$ (probably via the Stark shift), and as such model the Hamiltonian by

$$\begin{aligned} \mathcal{H} = & \sum_{j=1}^N [(\omega_j + \delta_j)(\sigma_j^+ \sigma_j^- + a_j^\dagger a_j) + \beta_j(\sigma_j^+ a_j + \sigma_j^- a_j^\dagger)] \\ & - \kappa \sum_{\langle i,j \rangle} a_i^\dagger a_j, \end{aligned} \quad (29)$$

where the set $\{\delta_1, \delta_2, \dots, \delta_N\}$ are chosen from a normal distribution with zero mean and standard deviation ς . For a fixed number of cavities and fixed ς , we calculate 1000 sets each of boundaries above $l=0$ to below $l=2N$, and take the mean of the results. Results are shown in Fig. 9(b).

One can see by comparing Figs. 9(a) and 9(b) that disorder and temperature produce qualitatively the same results. However, these disorder effects can only be calculated up to four cavities due to the limitations of computing resources, and the temperature analysis is only valid for large numbers of cavities. Hence the two techniques cannot be compared directly. If the exact diagonalization technique could be extended to a larger number of cavities, it could be compared quantitatively with disorder, matching properly the standard deviation with the effective temperature T .

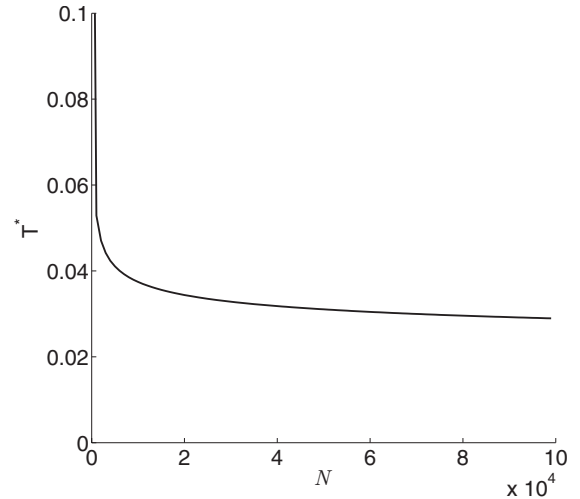


FIG. 10. How T^* , the temperature at which the top boundary of the first group in Fig. 9(a) meets the boundary of the second group, changes as a function of the number of cavities.

If one envisions Fig. 9(a) as temperature increases even further, there will be some temperature T^* such that the top line from the bottom group (corresponding to $l=N-2$) will meet the bottom line of the top group (corresponding to $l=N+1$). We examine T^* as a function of the number of cavities, and find that this is given by

$$T^* = (2 - \sqrt{2})[\Gamma(N-2) + \Gamma(N+2) - \Gamma(N-1) - \Gamma(N+1)]^{-1}, \quad (30)$$

where $\Gamma(l') = l' \frac{\partial S}{\partial l} \Big|_{l=l'}$. This function is plotted in Fig. 10. T^* appears to converge to a constant, nonzero temperature as $N \rightarrow \infty$.

V. CONCLUSIONS

In this paper we present an intensive analysis of the Jaynes-Cummings-Hubbard model using the exact diagonalization technique—studying the phase diagrams via the expectation value of the total number of excitations. We examine various topologies of small networks of cavities, and compare this work with the infinite cavity mean-field approximation. We find good agreement in all topologies. We study the effective model temperature, and compare this qualitatively with disorder in the photon energy of the exact JCH, and also find good agreement.

ACKNOWLEDGMENTS

The authors would like to acknowledge useful discussions with Z. E. Evans, A. M. Stephens, and C.-H. Su. A.D.G. and L.C.L.H. acknowledge the Australian Research Council for financial support (Projects No. DP0880466 and No. DP0770715, respectively). This work was supported in part by the Australian Research Council, the Australian Government and by the U.S. National Security Agency, and the U.S. Army Research Office under Contract No. W911NF-04-1-0290.

- [1] J. Hubbard, Proc. R. Soc. London, Ser. A **276**, 238 (1963).
- [2] M. P. A. Fisher, P. B. Weichman, G. Grinstein, and D. S. Fisher, Phys. Rev. B **40**, 546 (1989).
- [3] A. D. Greentree, S. G. Schirmer, F. Green, L. C. L. Hollenberg, A. R. Hamilton, and R. G. Clark, Phys. Rev. Lett. **92**, 097901 (2004).
- [4] M. Freedman, C. Nayak, and K. Shtengel, Phys. Rev. Lett. **94**, 066401 (2005).
- [5] D. Jaksch, C. Bruder, J. I. Cirac, C. W. Gardiner, and P. Zoller, Phys. Rev. Lett. **81**, 3108 (1998).
- [6] M. Greiner, O. Mandel, T. Esslinger, T. W. Hänsch, and I. Bloch, Nature (London) **415**, 39 (2002).
- [7] V. W. Scarola and S. DasSarma, Phys. Rev. Lett. **95**, 033003 (2005).
- [8] M. J. Hartmann, F. G. S. L. Brandão, and M. B. Plenio, Nat. Phys. **2**, 849 (2006).
- [9] A. D. Greentree, C. Tahan, J. H. Cole, and L. C. L. Hollenberg, Nat. Phys. **2**, 856 (2006).
- [10] D. Rossini and R. Fazio, Phys. Rev. Lett. **99**, 186401 (2007).
- [11] N. Na, S. Utsunomiya, L. Tian, and Y. Yamamoto, Phys. Rev. A **77**, 031803(R) (2008).
- [12] D. G. Angelakis, M. F. Santos, and S. Bose, Phys. Rev. A **76**, 031805(R) (2007).
- [13] M. J. Hartmann, F. G. S. L. Brandão, and M. B. Plenio, New J. Phys. **10**, 033011 (2008).
- [14] A. Imamoğlu, H. Schmidt, G. Woods, and M. Deutsch, Phys. Rev. Lett. **79**, 1467 (1997).
- [15] L. Tian and H. J. Carmichael, Phys. Rev. A **46**, R6801 (1992).
- [16] K. M. Gheri, W. Alge, and P. Grangier, Phys. Rev. A **60**, R2673 (1999).
- [17] A. D. Greentree, J. A. Vaccaro, S. R. de Echaniz, A. V. Durrant, J. P. Marangos, J. Opt. B: Quantum Semiclassical Opt. **2**, 252 (2000).
- [18] S. Rebić, A. S. Parkins, and S. M. Tan, Phys. Rev. A **65**, 063804 (2002).
- [19] K. M. Birnbaum, A. Boca, R. Miller, A. D. Boozer, T. E. Northup, and H. J. Kimble, Nature (London) **436**, 87 (2005).
- [20] B. Dayan, A. S. Parkins, T. Aoki, E. P. Ostby, K. J. Vahala, and H. J. Kimble, Science **319**, 1062 (2008).
- [21] E. T. Jaynes and F. W. Cummings, Proc. IEEE **51**, 89 (1963).
- [22] K. Sheshadri, H. R. Krishnamurthy, R. Pandit, and T. V. Ramakrishnan, Europhys. Lett. **22**, 257 (1993).
- [23] D. van Oosten, P. van der Straten, and H. T. C. Stoof, Phys. Rev. A **67**, 033606 (2003).
- [24] H.-J. Lee and R. Bulla, Eur. Phys. J. B **56**, 199 (2007).
- [25] K. Sengupta and N. Dupuis, Phys. Rev. A **71**, 033629 (2005).
- [26] M. J. Hartmann and M. B. Plenio, Phys. Rev. Lett. **100**, 070602 (2008).
- [27] S. Sachdev, *Quantum Phase Transitions* (Cambridge University Press, Cambridge, UK, 1999).
- [28] P. Olivero *et al.*, Adv. Mater. (Weinheim, Ger.) **17**, 2427 (2005).
- [29] S. Tomljenovic-Hanic, M. J. Steel, C. M. de Sterke, and J. Salzman, Opt. Express **14**, 3556 (2006).
- [30] A. D. Greentree *et al.*, J. Phys.: Condens. Matter **18**, S825 (2006).
- [31] A. Wallraff, D. I. Schuster, L. Frunzio, R. S. Huang, J. Majer, S. Kumar, S. M. Girvin, and R. J. Schoelkopf, Nature (London) **431**, 162 (2004).
- [32] D. I. Schuster *et al.*, Nature (London) **445**, 515 (2007).
- [33] M. Trupke, E. A. Hinds, S. Eriksson, E. A. Curtis, Z. Moktadir, E. Kukharenska, and M. Kraft, Appl. Phys. Lett. **87**, 211106 (2005).
- [34] D. E. Chang, A. S. Sørensen, P. R. Hemmer, and M. D. Lukin, Phys. Rev. Lett. **97**, 053002 (2006).
- [35] M. J. Hartmann, F. G. S. L. Brandão, and M. B. Plenio, Phys. Rev. Lett. **99**, 160501 (2007).
- [36] E. K. Irish, C. D. Ogden, and M. S. Kim, Phys. Rev. A **77**, 033801 (2008).
- [37] F. M. Hu, L. Zhou, T. Shi, and C. P. Sun, Phys. Rev. A **76**, 013819 (2007).
- [38] H. Hellmann, *Einführung in die Quantenchemie* (Deuticke, Leipzig, 1937).
- [39] R. P. Feynman, Phys. Rev. **56**, 340 (1939).
- [40] N. S. Witte, L. C. L. Hollenberg, and Zheng Weihong, Phys. Rev. B **55**, 10412 (1997).
- [41] D. J. Amit and Y. Verbin, *Statistical Physics: An Introductory Course* (World Scientific, River Edge, NJ, 1999).